View Article Online / Journal Homepage / Table of Contents for this issue
Dynamic Article Links

CrystEngComm

Cite this: *CrystEngComm*, 2012, **14**, 2190

www.rsc.org/crystengcomm

PAPER

Published on 19 January 2012. Downloaded by National Chiao Tung University on 28/04/2014 23:26:32.

The evolution of Ge nanostructures growth on silicon substrate by reduction of GeO_2†

Hung-Chi Wu,[a] Hsin-Tien Chiu[b] and Chi-Young Lee*[ac]

Received 5th November 2011, Accepted 21st November 2011
DOI: 10.1039/c2ce06485e

Various shaped and sized Ge nanostructures were obtained by reducing GeO_2 powder under a H_2 atmosphere in a high-temperature tubular furnace. At a high depositing temperature region, crystalline Ge film was epitaxially grown on a silicon substrate. Jellyfish-like Ge/SiO_2NWs composite structures were obtained next to germanium epitaxial film grown by Ge-catalyzed vapor–liquid–solid phase segregation mechanism. In addition, at the lower depositing temperature zones, Ge nanowires with various morphologies were formed owing to the temperature and concentration gradient by oxide-assisted vapor–solid mechanism and Ostwald ripening.

Introduction

One-dimensional nanowires (NWs) have attracted great attention and also stimulated extensive interest in recent years because of their unique properties and potential applications as building blocks that can be incorporated into modern nanoscaled electronic and photonic devices.[1–3] Up to now, a diverse variety of NWs (such as group IV, III–V, II–VI, carbides, silicides, nitrides and oxides) has been successfully synthesized. Among these materials, Ge and SiO_2 in NW structured have attracted greater attention for several years. Because Ge possesses a high carrier mobility, a larger excitonic Bohr radius, a strong absorption band in the near-infrared range, and a high refractive index;[4–6] and SiO_2 has an intense and stable blue light emission at room temperature.[7] There are many approaches for fabricating NWs including laser ablation,[8,9] molecular beam epitaxy,[10] template-based method,[11] chemical vapor deposition (CVD),[12] thermal evaporation,[8,9,13] and solvothermal routes.[14,15] Among these techniques, CVD and thermal evaporation techniques based on a vapor phase transport mechanism have been extensively employed for its simple and low-cost approaches which will provide large quantity and high crystalline quality products.

Metal catalysts have been commonly used to assist and control the NW growth. Nowadays, "Au" is the common metal catalyst used for NW synthesis due to its chemical inertness, thermal stability and ability to form an eutectic alloy at low temperature.[16,17] Unfortunately, Au is a deep level impurity that can highly detriment the performance of electronic devices and may need to be eliminated,[18,19] or to find a suitable alternative catalyst (such as Ga, Ge, Bi, and In),[9,20–24] and furthermore, to grow NWs by a self-catalytic or non-catalytic method,[25–29] and consequently to promote NW-based device technologies.

Previously, we reported the formation of several GeNWs without a foreign metal catalyst in a single run of an experiment, and also suggested a possible formation pathway.[30] However, questions about how the GeNWs form need to be elucidated. In this report, we discuss four successive regions that are prepared by CVD with the source material, GeO_2, and Si substrates under a H_2 atmosphere. The sequence of the four successive regions, that were obtained in a single run of an experiment, from the front side to the rear end of the downstream tube side are single-crystalline Ge film, Ge-particle/SiO_2NW-tails assembled structures, and two sizes GeNWs grown without external metal catalysts: one is with a thin diameter and droplet-like tip end, and the other is with a thick diameter and sidewall chunks/nodules. These areas gradually change as the temperatures, chemical compositions and concentrations of reactive species were different. Finally, a possible formation mechanism for all the obtained products is proposed.

Experimental

Synthesis

The Ge film, GeNWs and SiO_2NWs were synthesized in a single run of an experiment by the CVD method in a horizontal hot-wall quartz tubular reactor comprising a pumping system, a reaction chamber heated by a tubular furnace. Several silicon strips were cleaned in acetone and used as substrates. The source

[a]*Department of Materials Science and Engineering, National Tsing Hua University, Hsinchu, Taiwan, 30013, R. O. C. E-mail: cylee@mx.nthu.edu.tw*
[b]*Department of Applied Chemistry, National Chiao Tung University, Hsinchu, Taiwan, 30010, R. O. C*
[c]*Center for Nanotechnology, Materials Science, and Microsystems, National Tsing Hua University, Hsinchu, Taiwan, 30013, R. O. C*

† Electronic supplementary information (ESI) available: TEM image of a Ge-particle/SiO_2NW-tails assembled structure and its corresponding room-temperature CL spectrum; TEM image of a Ge nanowire in zone III and its fast Fourier transform; TEM image of a Ge nanowire in zone IV. See DOI: 10.1039/c2ce06485e

 This journal is © The Royal Society of Chemistry 2012

View Article Online

Published on 19 January 2012. Downloaded by National Chiao Tung University on 28/04/2014 23:26:32.

material, GeO_2 powder (0.5 g, 99.999%, Alfa Aesar), was placed in an alumina boat in the high temperature zone while the substrates were placed in the low temperature zone, downstream of the reaction chamber. Before heating, the reaction chamber was pumped into a vacuum pressure of 10^{-3} torr. Then the carrier gas, H_2, was introduced into the reaction chamber at a flow rate of 90 sccm (standard cubic centimetres per minute). The high-temperature zone was maintained at 1100 °C with the chamber pressure of about 15–20 torr for 6 h.

Characterization

The as-synthesized samples were studied by X-ray diffraction (Bruker D8) using a Cu-Kα radiation and micro-Raman spectroscopy (Lab Raman HR800, Jobin Yvon) using a He–Ne laser with a wavelength of 632.8 nm. The surface morphology and crystallinity of the as-synthesized samples were observed under a scanning electron microscope (SEM, JEOL - 6500F) and a transmission electron microscope (TEM, JEOL - 3000F, 2100F, and 2010) respectively. The chemical compositions of the products were analyzed by energy dispersive spectroscopy (EDS) that is equipped on SEM and TEM. Cathodoluminescence (CL) experiments were carried out in room temperature using a Gatan Mono CL system equipped with SEM and the optical signal was measured by a cooling PMT detector. In addition, there are two different types of samples prepared for the TEM imaging: One was made by depositing a solution of NWs (scraped down and dispersed in ethanol under ultrasound) onto a carbon film copper grid, while the other was peeling off the product from the substrate by using a Ga dual beam system (FEI - Nova 200) which includes a focused ion beam and an electron beam.

Results and discussion

Fig. 1 shows the four distinctive zones on silicon wafer from the downstream side of the chemical vapor deposition by using GeO_2 as a precursor in the hydrogen atmosphere. In front of the downstream side, the first region is a silver-gray Ge film (zone I, ~1000–920 °C), the second region is composed of numerous "Ge-particle/SiO_2NW-tails" jellyfish-like composite structures (zone II, ~920–790 °C), the third region is formed by spherically tipped thin GeNWs (zone III, ~790–680 °C) and the last region is full of thick GeNWs with/without chunks or nodules on their sidewall (zone IV, ~680–600 °C). The characterizations and formation of each region are described in the following sections.

At the high temperature range (1000–920 °C), a silver-gray Ge film deposited on the Si substrate was observed (as shown in Fig. 2a). According to the cross-sectional SEM images, the thickness of this film decreased gradually from 10 μm to 0.2 μm from up- to down-stream side. Previous characterizations[31] revealed that this silver-gray film is a single-crystalline Ge layer epitaxially grown on the crystalline silicon substrate with an intermediate Ge_xSi_{1-x} ($0 < x < 1$) buffer layer, however, the interface between this Ge film and Si substrate is very rough (as shown in Fig. 2b). The XRD and Raman studies in Fig. 2c–d also show that the film possesses a high crystallinity of Ge, while the Ge_xSi_{1-x} buffer layer becomes a significant component in the downstream part of the film.

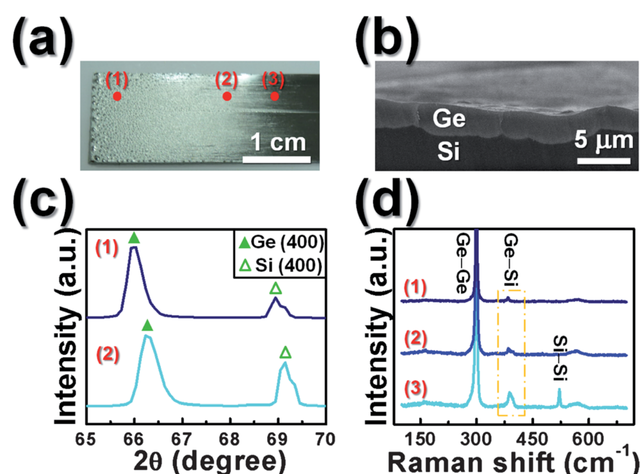

Fig. 2 (a) Optical photography of the as-synthesized specimen from zone I; (b) cross-sectional SEM image of the silver-gray Ge film; (c) XRD patterns and (d) Raman spectra from the corresponding regions in (a).

The following region, zone II in the temperature range of 920–790 °C, showed a colourful appearance of light blue, deep gray and cream yellow on the Si substrate. At the upstream side of this region, numerous entangled SiO_2NWs (10–60 nm in diameter) and Ge particles (50 nm–1 μm in diameter) randomly distributed on the substrate (Fig. 3a). In the middle of this region, numerous different sized jellyfish-like composite structures (each is with SiO_2NW hairs and a Ge round head) spread on the substrate, as shown in Fig. 3b–c. In this part, large jellyfish-like structures with large bundles of NWs (20–120 nm in diameter, 20 μm in length) and a large round particle (1–4 μm in diameter) stand closely on the substrate. Fig. 3d shows a single jellyfish-like structure, it clearly revealed that NWs with a hierarchical shape like hair-braids connecting to the lower hemisphere of the huge round particle, and the ends of NWs fused together forming thick wires as shown in the marked square in Fig. 3d. TEM/EDS analyses show that the upper hemisphere of the particles were

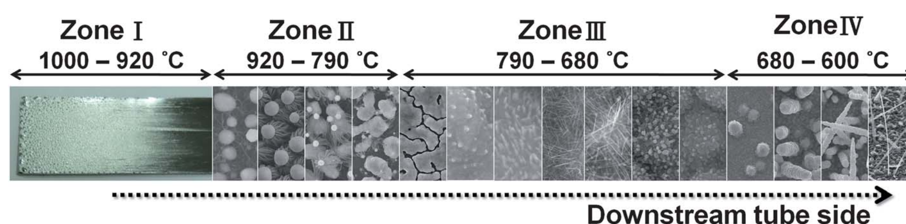

Fig. 1 Schematic diagram of position with corresponding temperature range of the four deposition zones inside the reaction tube. The morphologies of those as-synthesized products progressively changing in these zones are shown.

View Article Online

Published on 19 January 2012. Downloaded by National Chiao Tung University on 28/04/2014 23:26:32.

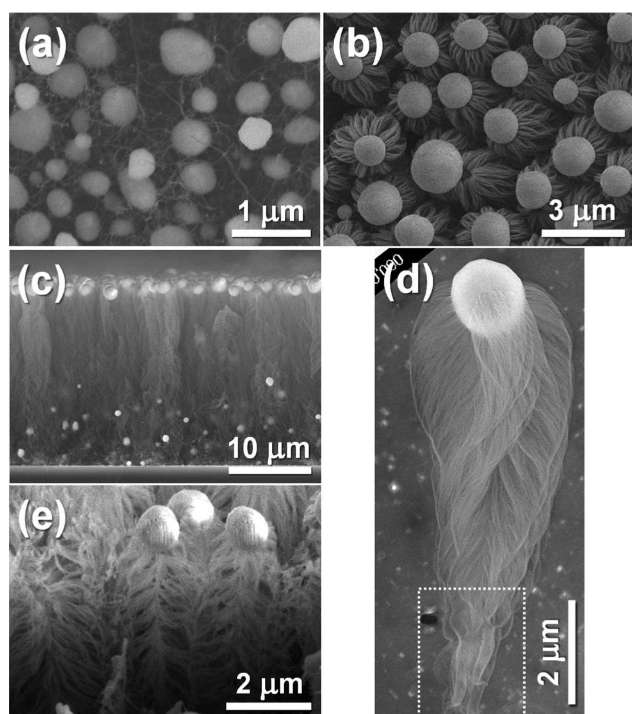

Fig. 3 SEM images of the as-synthesized products form the (a) front part and (b) middle part of zone II; (c) a cross-sectional image from (b); (d) a single Ge-particle/SiO_2NWs jellyfish-like structure; (e) a cross-sectional SEM image of the vertical dissected jellyfish-like structures.

composed of Ge and O (~90% and 10%), while the lower hemisphere of the particles were composed of Ge, O, and Si (~70%, 20% and 10%, respectively), and the NWs were composed of amorphous SiO_2 with traces of Ge (~1%). Further, a cross-sectional SEM image of the vertical dissected jellyfish-like structures (Fig. 3e) and a typical TEM image of a jellyfish-like structure (Fig. S1a†) revealed a fishbone-like organized SiO_2NWs constructing the tails. In addition, the jellyfish-like structures exhibited a strong blue light emission at 392 nm at room temperature CL measurement (Fig. S1b†). Jellyfish-like structures with a smaller head (500–100 nm) and shorter tails (2–0.5 μm in length) were obtained at lower temperature at the end of zone II (two places are shown in Fig. 4a–b). Fig. 4c shows the typical TEM image of the structure from Fig. 4b, and this structure is composed of several ribbons connected to a spherical head. The chemical compositions of the spherical-head and tailed-ribbons are similar to the compositions of jellyfish-like structures shown in Fig. 3b. In addition, the split of the tail was shown in the circled region in Fig. 4c. Fig. 4d shows a large-magnified TEM image and a SAED (selected area electron diffraction) pattern from the marked square in Fig. 4c. It indicates that these SiO_2 tails with many branches are amorphous. In addition, many Ge islands from separate distributions coalesced together were also observed underneath these jellyfish-like structures from up- to down-stream of zone II.

The third zone corresponds to the temperature range of 790–680 °C, showing that the morphology evolution from higher to lower temperature regions containing Ge islands, Ge islands with blisters on them, and Ge thin film with different sized and

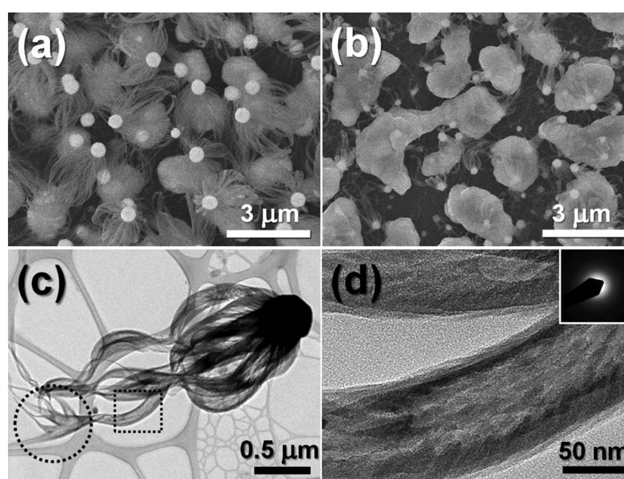

Fig. 4 (a)–(b) SEM images of the as-synthesized products form two areas of the downstream part of zone II; (c) typical TEM image from the structure in (b); (d) high-magnified image from marked square in (c), and the inset shows its corresponding SAED pattern.

shaped one dimensional Ge nanostructures on it, as shown in Fig. 5–6. SEM images show that the surface of Ge islands was smooth in the highest temperature region of zone III (Fig. 5a), then blistered (Fig. 5b), and sprouted NWs in the lower temperature region of zone III (Fig. 5c). Fig. 5d presents a cross-sectional TEM image of the Ge islands in Fig. 5a, the HR-TEM image from the indicated square area was shown in the upper inset and the lower inset is the SAED pattern from the point "a". From the TEM and SAED investigations, the Ge islands were polycrystalline and there was an oxide layer between the Ge islands and the Si substrate. At further lower temperature areas, thin and long NWs (~1 μm in length) without and with a droplet end on the Ge thin film were obtained, as shown in Fig. 6a–b. A TEM study (an example shown in Fig. S2a†) shows that these NWs were composed of a crystalline Ge core (6–15 nm in

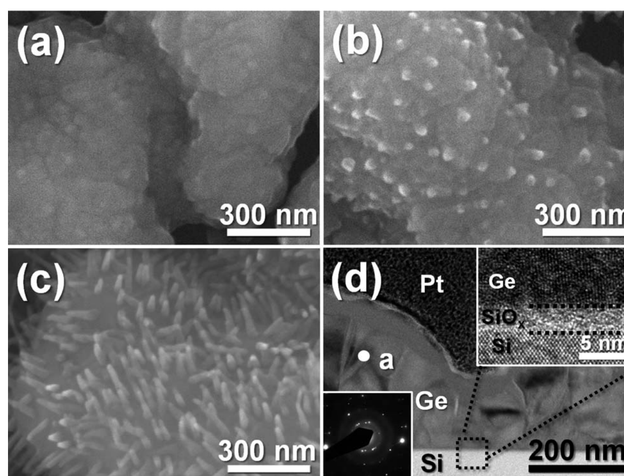

Fig. 5 (a)–(c) SEM images of the as-synthesized products progressively change form the front end of zone III; (d) a cross-sectional TEM image of the coalesced Ge island in (a), the upper inset shows the HR-TEM image from the indicated square area, and the lower inset shows the SAED pattern around the point a.

This journal is © The Royal Society of Chemistry 2012

Published on 19 January 2012. Downloaded by National Chiao Tung University on 28/04/2014 23:26:32.

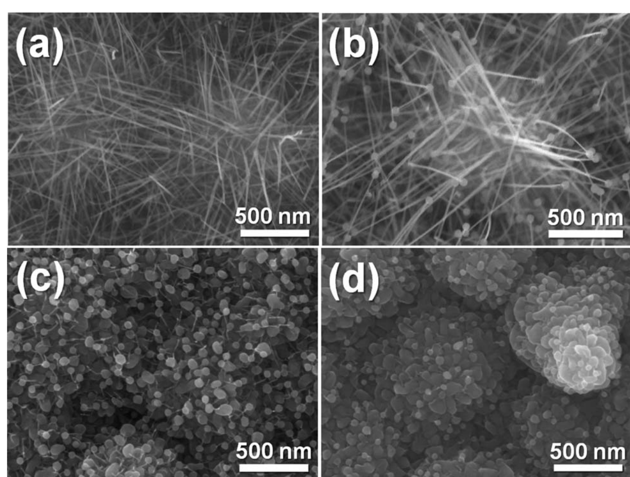

Fig. 6 (a)–(d) SEM images of the as-synthesized products progressively changed at the downstream part of zone III.

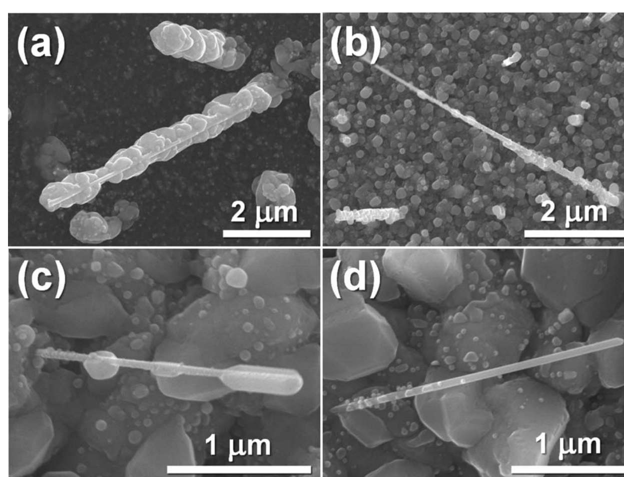

Fig. 8 (a)–(d) Four representative SEM images from the products in zone IV.

diameter) enclosed by an amorphous oxide shell (with a thickness 3–6 nm); in addition, a preferential growth orientation along either [112] or [110] direction was identified by examining several NWs. TEM image (Fig. S2b–c†) shows that the droplet was also composed of a Ge core and an amorphous shell. In the lowest temperature area of zone III, very thin NWs with a large drop end and bulged stacking by disks were obtained, as show in Fig. 6c–d.

Zone IV corresponds to the temperature range of 680–600 °C, Ge rods and NWs with different surface morphologies were obtained, as shown in Fig. 7–8. In the upstream region of this area, thick Ge rods with protuberances on their side wall were the major products (Fig. 7a, 8a). The thinner Ge rods with less protuberances and tapered end were obtained in the middle area of zone IV (Fig. 7b, 8b). At the end of this zone, straight and uniform GeNWs with smooth surfaces were shown, and their lengths were of ~0.5–5 μm and with the diameters of ~30–200 nm, as shown in Fig. 7c. According to TEM analyses (an example is shown in Fig. S3†), the growth directions of NWs obtained in zone IV were also along either [110] or [112] direction.

Based on the above observations, the morphologies, distribution, and density of the products vary gradually with positions in the close successive regions at the downstream tube side. These products were identified into four regions: first, in front of the downstream side, the formed product is a silver-gray Ge epilayer with a Ge_xSi_{1-x} buffer layer. The second region is composed of numerous Ge particles and SiO_2NWs, which was self-assembled into a jellyfish-like Ge/SiO_2NW composite structure, in addition, several Ge islands were observed underneath the jellyfish-like structures. The third region is oxide-sheathed GeNWs without/with droplet ends sprouted from the Ge film, and these wires progressively diminished and their tipped particles gradually enlarged, stacked, and finally formed a bulged film. The final region contains a different amount of chunks/nodules grown on the sidewall of GeNWs.

According to the composition and morphology of such a series of products and together with their formation conditions, the possible formation pathways and precursors for the four successive zones were proposed by the following sections: At the high temperature regions (1100 °C), GeO_2 powder (melting point: 1086 °C) was reduced by H_2 resulting in the formation of Ge, different reducing forms of germanium oxide (GeO_y, $0 < y < 2$), and H_2O gaseous precursors, and these vapors are transported by the carrier gas to the following lower temperature regions. In zone I, GeO_y and H_2O could be the etching agent for etching the smooth silicon surface to become an undulated surface (Fig. 2b), meanwhile Ge (in GeO_y) would take the position of Si resulting in the formation of Ge layers on silicon. The formed graded Ge_xSi_{1-x} buffer layer accounted for the accommodation of the lattice mismatch between Si and Ge. Then, the thick Ge layer formed above the buffer layer by deposition of the Ge vapor.[31] In addition, while the previous GeO_y and H_2O reacted with the silicon surface, active silicon oxide species were generated[20–22] and flowed into the subsequent region.

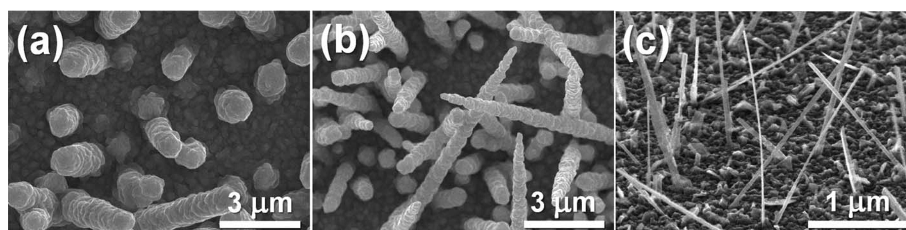

Fig. 7 (a)–(c) SEM images of the as-synthesized products progressively changed form zone IV.

View Article Online

Published on 19 January 2012. Downloaded by National Chiao Tung University on 28/04/2014 23:26:32.

Ge-particle/SiO_2NW-tails jellyfish-like composite structures in zone II are evidence of the existence of silicon oxide species as a precursor in this area. Such a jellyfish-like structure has been observed in the Ga- and Ge-catalyzed growth of silicon oxide nanowire assemblies.[9,20–22] Based on the growth models proposed by previous researches,[9,20–22] the jellyfish-like composite structure could be explained by an extended Ge-catalyzed vapor–liquid–solid (VLS) growth mechanism as follows: while the Ge vapor deposited on substrate as liquid clusters, and the Ge clusters would absorb the previous gaseous silicon oxide species, then forming a germanium-silicon oxide droplet-shaped solution. With the instantaneously massive feeding of silicon oxide species from zone I, the concentration of silicon oxide species in the solution became supersaturated, and the silicon oxide species will segregate and precipitate from the solution to form many nucleation sites on the lower hemisphere surface of the germanium–silicon oxide droplet-shaped solution, and then initiating the growth of the SiO_2 nanowires. The germanium-silicon oxide droplet solution is then pushed away from the substrate by the growing SiO_2NWs. From the dissected SEM image (Fig. 3e) and TEM images (Fig. 4c and S1a†), the SiO_2NWs with a fishbone-like branching growth coupled with a splitting growth resulted in the formation of Ge-head/SiO_2NW-tails jellyfish-like composite structures. Because of the concentration of reactive species and temperature gradient along the axial direction of the tubular reaction chamber, the dimensions of the jellyfish-like composite structures decreased from up- to down-stream areas in zone II (from Fig. 3b to Fig. 4a–b). In addition, as the silicon oxide species were exhausted to form SiO_2 nanowires and the substrate temperature decreased, the deposited Ge droplets in the low temperature region fused to form Ge islands (underneath the jellyfish structures in Fig. 4a), and then coalesced together (Fig. 4b).

In the following two zones (zones III and IV), GeO_y and Ge (formed by reducing GeO_y) vapors are the major precursors inducing the formation of different sized Ge wires. In general, in the high temperature and high reagent concentration, thick or large amounts of wires/rods are formed as the major products in the upstream, and thin or dilute wires/rods are the major products in the downstream.

In zone III, GeO_y vapor is the major precursor to induce the formation of GeNWs with an oxide shell. The GeO_y vapor was absorbed by the numerous active sites of the Ge island surface, to initiate the growth of nanowires (Fig. 5a–c). As to the following areas, the dimensions of the GeNWs shrank, and a homogeneous spherical Ge particle emerged and expanded at the tip of each NW as shown in Fig. 6b–d. Wires with a germanium droplet end formed by minimizing the surface energy are products similar to those from typical Ostwald ripening results.[32] A HR-TEM image (Fig. S2a†) of a GeNW shows that the NW is composed of a crystalline Ge core and covered a thick amorphous oxide shell. This core-shell structure can account for the phase segregation and separation processes of GeO_y, and further the GeNWs direction are along either [112] or [110], consistent with the features of oxide species (like SiO, GeO, and SnO) in the oxide-assisted vapor–solid growth mechanism.[8,9,33]

In zone IV, GeNWs with and without chunks or nodules on their sidewall were obtained as the major products. Although a considerable quantity of Ge (both Ge and GeO_y) had been exhausted in previous zones, the residual GeO_y can still be reduced by carrier gas (H_2) to form an extra amount of Ge vapor to achieve the posterior areas of the downstream tube side, and the additional reduced Ge vapor would be the precursor to provide the GeNWs growth. As we know, the concentration of reactive species is higher in the upstream region, thus wires/rods with several sidewalled chunks or nodules were obtained (Fig. 7a–b, 8a–c); while in the downstream region, the lower concentration of reactive species causes wires/rods with less nodules or small chunks on the sidewall (or without nodules and chunks on the sidewall) (Fig. 7c, 8d). The GeNWs obtained in this low temperature region with their tipped end are not appropriate for the conventional VLS growth process. On the other hand, based on the oxide-related precursors, the vapor phase transport dependent formation and the preferential growth direction along [112] or [110], strongly implied an oxide-assisted vapor–solid growth mechanism of GeNWs.[30] In addition, while a single-crystalline [100]-orientated Ge substrate was used, the sprouted GeNWs in zones III and IV revealed a clearly preferred orientation, as shown in Fig. 9a–b, and this will need a further investigation in the future.

Conclusions

In summary, four successive regions with single-crystalline Ge film, SiO_2 assembled nanowires with a large Ge particle at the tip, and Ge nanowires with different sizes and shapes were obtained by reducing GeO_2 powder in the H_2 atmosphere. In the high temperature region (zone I), single-crystalline Ge film was epitaxially grown on a crystal Si substrate with a buffer layer *via* Ge vapor deposition. Meanwhile the silicon substrates were etched to form the silicon oxide species which acted as the source of SiO_2 nanowires growth in zone II. And the jellyfish-like Ge/SiO_2NW structure formed by an extended Ge-catalyzed vapor–liquid–solid mechanism at about 920–790 °C exhibited a strong blue light emission at 392 nm. In the low-temperature regions (zones III and IV), Ge/GeO_y core-shell nanowires formed by phase segregation and separation *via* an oxide-assisted vapor–solid growth and Ge nanowires with chunks/nodules on the sidewall surface also grown by an oxide-assisted vapor–solid process. The different sized droplets on the Ge nanowire tip are similar to Ostwald ripening products. And a sidewall growth is a typical phenomenon of the vapor–solid growth mechanism.

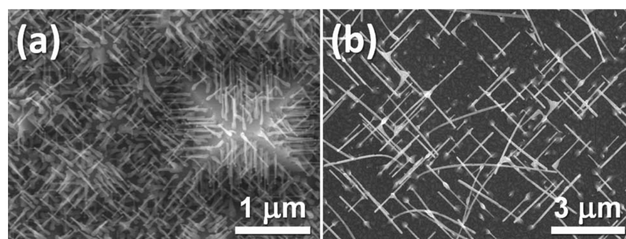

Fig. 9 SEM images of the as-synthesized products form (a) zone III and (b) zone IV by using [100]-oriented crystalline Ge strips as substrates.

 This journal is © The Royal Society of Chemistry 2012

View Article Online

Published on 19 January 2012. Downloaded by National Chiao Tung University on 28/04/2014 23:26:32.

Acknowledgements

The authors would like to thank Dr Hsueh-Shih Chen for consulting Ostwald ripening events, and Miss Shalini Jayakumar for grammatical editing, and the National Science Council of the Republic of China, Taiwan, for financially supporting this research under Contract No. NSC-96-2113-M-007-021 and NSC-99-2113-M-007-011.

Notes and references

1 Y. N. Xia, P. D. Yang, Y. G. Sun, Y. Y. Wu, B. Mayers, B. Gates, Y. D. Yin, F. Kim and Y. Q. Yan, *Adv. Mater.*, 2003, **15**, 353–389.
2 Y. Li, F. Qian, J. Xiang and C. M. Lieber, *Mater. Today*, 2006, **9**, 18–27.
3 P. J. Pauzauskie and P. D. Yang, *Mater. Today*, 2006, **9**, 36–45.
4 S. M. Sze and K. K. Ng, *Physics of Semiconductor Devices*, 3rd ed.; Wiley: New York, 2007.
5 B. Streetman and S. Banerjee, *Solid State Electronic Devices*, 6th ed.; Prentice Hall: Upper Saddle River, NJ, 2005.
6 L. Colace, G. Masini and G. Assanto, *IEEE J. Quantum Electron.*, 1999, **35**, 1843–1852.
7 D. P. Yu, Q. L. Hang, Y. Ding, H. Z. Zhang, Z. G. Bai, J. J. Wang, Y. H. Zou, W. Qian, G. C. Xiong and S. Q. Feng, *Appl. Phys. Lett.*, 1998, **73**, 3076–3078.
8 N. Wang, Y. H. Tang, Y. F. Zhang, C. S. Lee and S. T. Lee, *Phys. Rev. B: Condens. Matter Mater. Phys.*, 1998, **58**, 16024–16026.
9 J. Q. Hu, Y. Jiang, X. M. Meng, C. S. Lee and S. T. Lee, *Small*, 2005, **1**, 429–438.
10 W. Guo, M. Zhang, A. Banerjee and P. Bhattacharya, *Nano Lett.*, 2010, **10**, 3355–3359.
11 G. Z. Cao and D. W. Liu, *Adv. Colloid Interface Sci.*, 2008, **136**, 45–64.
12 H. K. Lin, H. A. Cheng, C. Y. Lee and H. T. Chiu, *Chem. Mater.*, 2009, **21**, 5388–5396.
13 T. Ghoshal, S. Biswas, S. Kar, A. Dev, S. Chakrabarti and S. Chaudhuri, *Nanotechnology*, 2008, **19**, 065606.
14 C. W. Peng, M. Richard-Plouet, T. Y. Ke, C. Y. Lee, H. T. Chiu, C. Marhic, E. Puzenat, F. Lemoigno and L. Brohan, *Chem. Mater.*, 2008, **20**, 7228–7236.
15 H. C. Wu, H. Y. Tsai, H. T. Chiu and C. Y. Lee, *ACS Appl. Mater. Interfaces*, 2010, **2**, 3285–3288.
16 R. S. Wagner and W. C. Ellis, *Appl. Phys. Lett.*, 1964, **4**, 89–90.
17 Y. Y. Wu and P. D. Yang, *J. Am. Chem. Soc.*, 2001, **123**, 3165–3166.
18 J. H. Woodruff, J. B. Ratchford, I. A. Goldthorpe, P. C. McIntyre and C. E. D. Chidsey, *Nano Lett.*, 2007, **7**, 1637–1642.
19 C. M. Hessel, A. T. Heitsch and B. A. Korgel, *Nano Lett.*, 2010, **10**, 176–180.
20 Z. W. Pan, Z. R. Dai, C. Ma and Z. L. Wang, *J. Am. Chem. Soc.*, 2002, **124**, 1817–1822.
21 Z. W. Pan, S. Dai, D. B. Beach and D. H. Lowndes, *Nano Lett.*, 2003, **3**, 1279–1284.
22 Z. J. Gu, F. Liu, J. Y. Howe, M. P. Paranthaman and Z. W. Pan, *Nanoscale*, 2009, **1**, 347–354.
23 C. Y. Yan and P. S. Lee, *J. Phys. Chem. C*, 2009, **113**, 2208–2211.
24 Y. Xiang, L. Y. Cao, S. Conesa-Boj, S. Estrade, J. Arbiol, F. Peiro, M. Heiss, I. Zardo, J. R. Morante, M. L. Brongersma and A. F. I. Morral, *Nanotechnology*, 2009, **20**, 245608.
25 Y. H. Yang, B. Wang and G. W. Yang, *Cryst. Growth Des.*, 2007, **7**, 1242–1245.
26 B. S. Kim, T. W. Koo, J. H. Lee, D. S. Kim, Y. C. Jung, S. W. Hwang, B. L. Choi, E. K. Lee, J. M. Kim and D. Whang, *Nano Lett.*, 2009, **9**, 864–869.
27 R. G. Hobbs, S. Barth, N. Petkov, M. Zirngast, C. Marschner, M. A. Morris and J. D. Holmes, *J. Am. Chem. Soc.*, 2010, **132**, 13742–13749.
28 N. Zaitseva, J. Harper, D. Gerion and C. Saw, *Appl. Phys. Lett.*, 2005, **86**, 053105.
29 C. A. Barrett, H. Geaney, R. D. Gunning, F. R. Laffir and K. M. Ryan, *Chem. Commun.*, 2011, **47**, 3843–3845.
30 H. C. Wu, T. C. Hou, Y. L. Chueh, L. J. Chen, H. T. Chiu and C. Y. Lee, *Nanotechnology*, 2010, **21**, 455601.
31 H. C. Wu, B. H. Lin, H. C. Chen, P. C. Chen, H. S. Sheu, I. N. Lin, H. T. Chiu and C. Y. Lee, *ACS Appl. Mater. Interfaces*, 2011, **3**, 2398–2401.
32 Z. A. Peng and X. G. Peng, *J. Am. Chem. Soc.*, 2001, **123**, 1389–1395.
33 J. Q. Hu, X. L. Ma, N. G. Shang, Z. Y. Xie, N. B. Wong, C. S. Lee and S. T. Lee, *J. Phys. Chem. B*, 2002, **106**, 3823–3826.